RESEARCH ARTICLE

A viral fusogen hijacks the actin cytoskeleton to drive cell-cell fusion

Ka Man Carmen Chan[1,2], Sungmin Son[2], Eva M Schmid[2], Daniel A Fletcher[1,2,3,4]*

[1]UC Berkeley–UC San Francisco Graduate Group in Bioengineering, Berkeley, United States; [2]Department of Bioengineering & Biophysics Graduate Group, University of California, Berkeley, Berkeley, United States; [3]Division of Biological Systems and Engineering, Lawrence Berkeley National Laboratory, Berkeley, United States; [4]Chan Zuckerberg Biohub, San Francisco, United States

Abstract Cell-cell fusion, which is essential for tissue development and used by some viruses to form pathological syncytia, is typically driven by fusogenic membrane proteins with tall (>10 nm) ectodomains that undergo conformational changes to bring apposing membranes in close contact prior to fusion. Here we report that a viral fusogen with a short (<2 nm) ectodomain, the reptilian orthoreovirus p14, accomplishes the same task by hijacking the actin cytoskeleton. We show that phosphorylation of the cytoplasmic domain of p14 triggers N-WASP-mediated assembly of a branched actin network. Using p14 mutants, we demonstrate that fusion is abrogated when binding of an adaptor protein is prevented and that direct coupling of the fusogenic ectodomain to branched actin assembly is sufficient to drive cell-cell fusion. This work reveals how the actin cytoskeleton can be harnessed to overcome energetic barriers to cell-cell fusion.

Introduction

Cell-cell fusion plays a critical role in the development of multicellular organisms, beginning with fertilization and continuing with formation of muscles, osteoclasts, and the placenta in mammals. Viral pathogens, including some members of poxvirus, paramyxovirus, herpesvirus, retrovirus, aquareovirus and orthoreovirus, cause infected cells to fuse with their neighbors, creating syncytia that contribute to disease pathology (***Compton and Schwartz, 2017***; ***Domachowske and Rosenberg, 1999***; ***Moss, 2006***; ***Smith et al., 2009***). While the basic steps of membrane fusion have been extensively investigated in the context of enveloped virus entry and SNARE-mediated intracellular vesicle fusion (***Südhof and Rothman, 2009***), the molecules and pathways responsible for cell-cell fusion are less well understood. The best studied cell-cell fusogens are those with similarities to enveloped viral fusogens, including syncytin-1 (placental syncytiotrophoblasts formation) (***Gong et al., 2005***; ***Renard et al., 2005***), Hap2 (conserved in eukaryotic gamete fusion) (***Fédry et al., 2017***; ***Feng et al., 2018***; ***Liu et al., 2008b***; ***Mori et al., 2006***; ***Valansi et al., 2017***; ***von Besser et al., 2006***), and Eff-1/Aff-1 (*C. elegans* epithelial fusion) (***Mohler et al., 2002***; ***Pérez-Vargas et al., 2014***; ***Sapir et al., 2008***; ***Shemer et al., 2004***; ***Zeev-Ben-Mordehai et al., 2014***).

A key feature of viral and cell-cell fusogens is their tall ectodomains, which in their metastable pre-fusion state typically extend more than 10 nm from the membrane. Since the plasma membrane of cells is densely decorated with glycoproteins and glycolipids that could sterically block membranes from getting close enough to fuse, the tall ectodomains of viral and cell-cell fusogens may allow them to reach across the membrane gap and anchor to the apposing membrane, involving insertion of a fusion peptide for Class I viral fusogens or a fusion loop for Class II (***Harrison, 2015***; ***Podbilewicz, 2014***). Once the fusogen links the two membranes, conformational changes cause the fusogen to fold back, pulling the two membranes into close contact and forming a stable post-fusion structure that promotes membrane fusion (***Bullough et al., 1994***; ***Chen et al., 1999***; ***Harrison, 2015***;

***For correspondence:** fletch@berkeley.edu

Competing interests: The authors declare that no competing interests exist.

Funding: See page 14

Received: 26 August 2019
Accepted: 08 May 2020
Published: 22 May 2020

Reviewing editor: Michael M Kozlov, Tel Aviv University, Israel

Ivanovic and Harrison, 2015; *Pancera et al., 2014*; *Podbilewicz, 2014*; *Sapir et al., 2008*; *Wilson et al., 1981*). This conformational change, together with fusogen oligomerization and local cooperativity, is believed to be sufficient to provide the energy required to overcome the repulsive hydration barrier, which prevents membranes from coming closer than ~2 nm (*Chernomordik and Kozlov, 2003*; *Harrison, 2015*; *Ivanovic and Harrison, 2015*; *Pérez-Vargas et al., 2014*; *Rand and Parsegian, 1989*).

However, in other instances of cell-cell fusion, transmembrane proteins required for fusion are short by comparison and do not appear to undergo conformational changes, raising the question of how they bring two plasma membranes into close contact (*Figure 1a*). One example is the reptilian orthoreovirus fusion protein p14, a non-structural, single-pass transmembrane protein, that is expressed after viral entry. One of seven members of the FAST family of reovirus fusion proteins discovered by Duncan and colleagues (*Ciechonska and Duncan, 2014*; *Corcoran and Duncan, 2004*; *Dawe and Duncan, 2002*; *Duncan et al., 1995*; *Duncan et al., 2004*; *Guo et al., 2013*; *Kim et al., 2015*; *Racine et al., 2009*; *Shmulevitz et al., 2004*; *Shmulevitz and Duncan, 2000*; *Wilcox and Compans, 1982*), p14 has a membrane-disruptive ectodomain that is necessary to drive cell-cell fusion but extends only 0.7–1.5 nm from the plasma membrane (*Corcoran et al., 2004*; *Corcoran et al., 2006*). This short ectodomain has minimal secondary structure but is sufficient to disrupt opposing membranes either when added as a soluble fragment or when bare liposomes containing p14 are brought into close apposition through divalent cations (*Corcoran et al., 2004*; *Top et al., 2005*). However, cell surfaces are crowded with proteins that sterically block close apposition, and it is unclear how p14 overcomes the energetic barrier of cell surface protein crowding, as well as the ~2 nm repulsive hydration barrier, to drive cell-cell fusion (*Chernomordik and Kozlov, 2003*; *Harrison, 2015*; *Rand and Parsegian, 1989*). Yet, expression of p14 alone in cultured cells is sufficient to drive fusion with neighboring naïve cells (*Corcoran and Duncan, 2004*; *Duncan et al., 2004*).

To address the question of how p14 promotes close contact between cells and drives membrane fusion, we studied cell-cell fusion in HEK293T cells transiently expressing p14. We found that p14 drives cell-cell fusion by hijacking the host cell actin cytoskeleton. Using a phosphorylation-dependent motif in its cytoplasmic domain, p14 triggers N-WASP-mediated assembly of branched actin, directly coupling actin assembly with a short membrane-disruptive ectodomain. This work suggests that energetic barriers to cell-cell fusion can be overcome by harnessing force generated from local actin assembly, and it points to an alternate means of promoting cell-cell fusion in processes where tall fusogens have not been identified.

Results

Expression of p14 in HEK293T cells caused the cells to fuse with neighboring wild-type and p14-expressing cells, forming large multinucleated syncytia over the course of 24 hr (*Figure 1b*, *Video 1*), like previous reports for other cell types (*Corcoran and Duncan, 2004*). Partial cleavage of the p14 cytoplasmic tail, which also occurs during reptilian orthoreovirus infection (*Top et al., 2009*), liberates the C-terminus mCherry fluorescent tag from the transmembrane protein and serves as a convenient cytoplasmic marker of p14-expressing cells (*Figure 1b*, *Figure 1—figure supplement 1a,b*, and *Video 2*). At 12 hr post transfection, 5% of p14-expressing cells had 3 or more nuclei. At 24 hr post transfection, 34% of p14-expressing cells had 3 or nuclei (*Figure 1c and d*). In comparison, at 24 hr post transfection, no multinucleated cells were seen in cells transfected with mCherry alone (*Figure 1—figure supplement 1c*).

To quantify cytoplasmic mixing during p14-mediated cell-cell fusion in a high-throughput manner, we expressed the two halves of splitYFP in two populations of HEK293T cells and mixed the cells together. When fusion between cells of the two populations occurred, the two halves of splitYFP self-associated in the mixed cytoplasm and fluoresced, allowing quantification by a plate reader (*Figure 1e*, and *Figure 1—figure supplement 1d and e*). Repeating the cell-cell fusion experiments above, the increase in YFP intensity in p14-expressing cells between 12 hr and 24 hr post transfection compared well with the increase in the percent of multinucleated cells, as quantified by counting nuclei (*Figure 1f*). Since YFP intensity is dependent on the percent of HEK293T cells expressing the two halves of splitYFP, the resultant YFP intensity was normalized to that of p14 WT and referred to as fusion index.

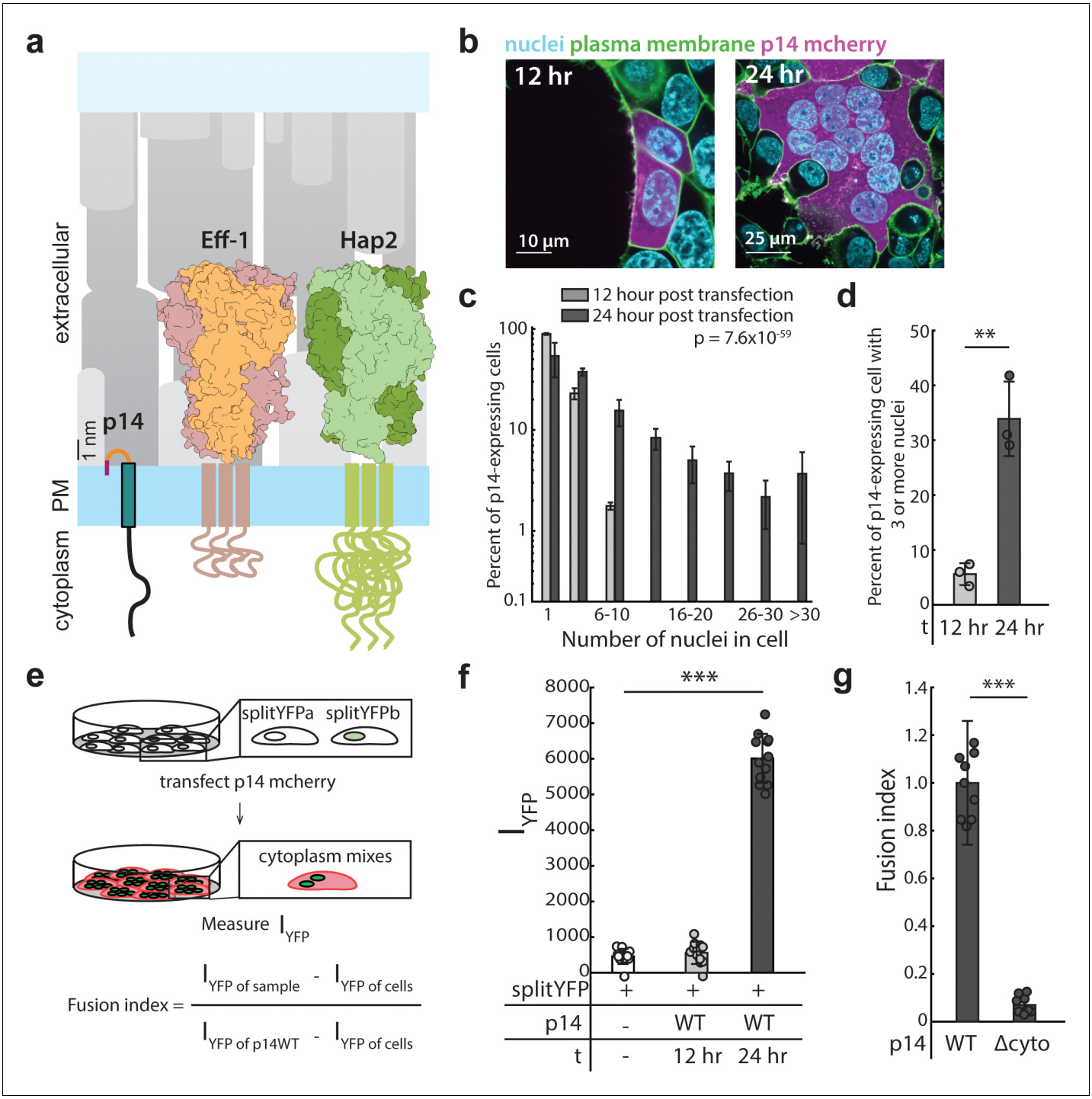

Figure 1. Expression of p14 drives cell-cell fusion and is quantified with a splitYFP fluorescent assay. (**a**) Schematic of fusion-associated small transmembrane protein, p14, in proportion to post-fusion trimeric structure of cell-cell fusogens, Eff-1 (PDB:4OJC) and Hap2 (PDB: 5MF1), on the plasma membrane. (**b**) Expression of p14 in HEK293T cells drives cell-cell fusion forming large multinucleated cells that increases size and number of nuclei over time. (**c**) Average nuclei count of HEK293T cells expressing p14 at 12 hr and 24 hr. P-values are ks-test and error bars represent standard deviation from 3 independent transfections (See also ***Figure 1—source data 1***). (**d**) Percent of p14 expressing nuclei in cells with 3 or more nuclei at 12 hr and 24 hr. P-values are two-tailed, two-sample Student's t-test where ** = p<0.01, and error bars represent standard deviations from 3 independent transfections (**e**) Schematic of the splitYFP fluorescence assay to quantify cell-cell fusion. $I_{YFP\ of\ sample}$ is the YFP fluorescence intensity of the sample, $I_{YFP\ of\ sample}$ is the YFP fluorescence intensity of the non-transfected cells, and $I_{YFP\ of\ sample}$ is the YFP fluorescence intensity of cells transfected with p14 WT. (**f**) Average YFP fluorescence intensity of HEK293T cells expressing p14 at 12 hr and 24 hr with error bars representing standard deviations from 3 independent transfections of 3 wells each. P-values are two-tailed, two-sample Student's t-test where *** = p<0.001 (See also ***Figure 1—figure***

Figure 1 continued on next page

Figure 1 continued

supplement 1c, (d). (**g**) Average fusion index of p14 cytoplasmic truncation mutant with error bars representing standard deviations from 3 independent transfections of 3 wells each. P-values are two-tailed, two-sample Student's t-test where *** = p<0.001 (See also ***Figure 1—figure supplement 1e, (f)***.

The online version of this article includes the following source data and figure supplement(s) for figure 1:

Source data 1. Excel Spreadsheet of counts and distribution for p14-expressing HEK293T cells at 12 hr and 24 hr post transfection for ***Figure 1c and d***.

Figure supplement 1. Characterization of p14 cytoplasmic tail cleavage and the splitYFP cell-cell fusion assay.

Figure supplement 1—source data 1. Excel Spreadsheet of surface biotinylation of p14-WT-GFP and p14-Δcyto-GFP for ***Figure 1—figure supplement 1h***.

While the ectodomain of p14 is shorter than typical viral fusogens, its cytoplasmic domain is comparatively long (68 amino acids). To determine how the cytoplasmic domain of p14 might be involved in cell-cell fusion, we first truncated Q70-I125 (p14 Δcyto), retaining a polybasic motif needed for trafficking to the plasma membrane (***Parmar et al., 2014***). Although p14 Δcyto was properly trafficked to the plasma membrane (***Figure 1—figure supplement 1f,g and h***), cell-cell fusion was abrogated (***Figure 1g***, and ***Figure 1—figure supplement 1i***). This is consistent with previous findings (***Corcoran and Duncan, 2004***), suggesting that p14 may be interacting with cellular components through its cytoplasmic tail to enable cell-cell fusion.

We next investigated whether post-translational modification of the cytoplasmic tail of p14 might play a role in cell-cell fusion. The p14 cytoplasmic tail is mostly disordered but has several tyrosines that could be phosphorylated (***Figure 2a***, and ***Figure 2—figure supplement 1a***). To determine if these tyrosines are indeed phosphorylated, we immunoprecipitated p14 and probed with an anti-phosphotyrosine antibody, which confirmed p14 phosphorylation (***Figure 2b***). Next, we mutated each predicted tyrosine to phenylalanine (Y59F, Y77F, Y96F, Y100F, Y116F) and found that only one mutation (Y116F) decreased cell-cell fusion (***Figure 2c*** and ***Figure 2—figure supplement 1b***). We then used NetPhos3.1 and Scansite 4.0 to analyze the cytoplasmic tail of p14, and they predicted that Y116 is phosphorylated by c-src kinase (***Figure 2d***; ***Blom et al., 2004***; ***Obenauer et al., 2003***). To test this prediction, we mutated all other predicted phosphotyrosines of p14 to phenylalanine (YEY; Y59F, Y77F, Y96F, Y100F) and co-expressed it with constitutively active c-src mutant (CA c-src; Y527F). Y116 phosphorylation subsequently increased, indicating c-src phosphorylates p14 (***Figure 2e***). Consistent with this, Y116 phosphorylation was also increased when tyrosine phosphatases were broadly inhibited by addition of pervanadate (***Figure 2e***). Finally, to confirm that c-src is sufficient to phosphorylate Y116, we carried out a modified *in vitro* kinase assay using a peptide including Y116 (Y116-N121), along with CA c-src and kinase dead c-src (KD c-src; Y527F/K295R) mutants immunoprecipitated from HEK239T cells (***Figure 2—figure supplement 1c and d***). We found that CA c-src was sufficient to phosphorylate p14 cytoplasmic tail peptide, but KD c-src was not (***Figure 2f***), showing that c-src kinase is sufficient to phosphorylate Y116 *in vitro*. To verify this in live-cells, we expressed p14 WT in mouse embryonic fibroblasts lacking src, yes, and fyn kinase (SYF), as well as SYF cells supplemented with c-src (SYF + c-src). Despite lower transfection efficiency and reduced cell-cell fusion compared to HEK239T cells, SYF + c-src cells fused more than SYF cells (***Figure 2g***). Altogether, this demonstrates that c-src phosphorylates Y116 in the p14 cytoplasmic tail to drive cell-cell fusion.

To determine which cellular components could be interacting with p14 upon phosphorylation, we used the Eukaryotic Linear Motif (ELM) prediction tool to identify potential binding motifs (***Dinkel et al., 2016***). ELM predicted that phosphorylated Y116 binds to the SH2 domain

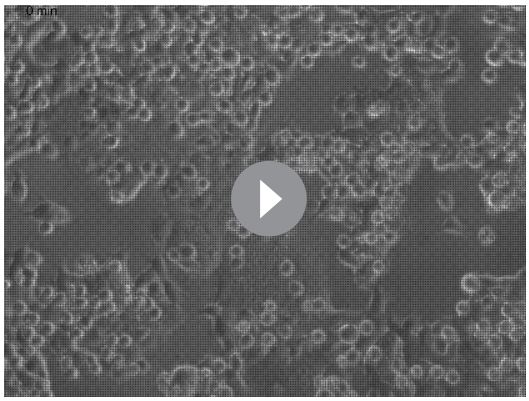

Video 1. Phase contrast timelapse of HEK293T cells expressing p14 WT showing extensive syncytium formation.
https://elifesciences.org/articles/51358#video1

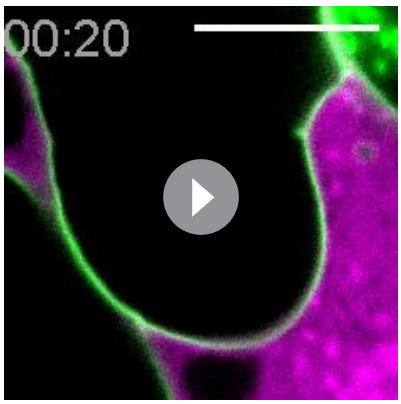

Video 2. Confocal timelapse of a HEK293T expressing p14-mcherry (magenta) fusing with a WT HEK293T cell that appears dark. Plasma membrane is marked with gpi-anchored pHluorin (green). Scale bar is 5 µm.
https://elifesciences.org/articles/51358#video2

of Grb2 as part of a Grb2 consensus-binding motif, YVNI (***Figure 3a***). To test this prediction, we carried out a co-immunoprecipitation assay and confirmed that p14 binds to Grb2 (***Figure 3b***). To determine if Grb2 binding is necessary for p14-mediated cell-cell fusion, we introduced two point mutations that disrupt the predicted Grb2 binding site both individually (Y116F, N118A) and together (FVAI; Y116F/N118A) (***Figure 3b***). While trafficking to the plasma membrane was intact, all three mutants severely attenuated cell-cell fusion (***Figure 3c***, ***Figure 3—figure supplement 1a,b and c***), suggesting that Grb2 is important for p14-mediated fusion. To confirm that p14 is sufficient to recruit Grb2, we conjugated biotinylated p14 cytoplasmic tail peptide to streptavidin beads *in vitro* and incubated them with purified Grb2 fluorescently labeled with AF647 (***Figure 3—figure supplement 1d***). Consistent with our co-immunoprecipitation results, only phosphorylated Y116 bound to Grb2 (***Figure 3d***, and ***Figure 3—figure supplement 1e***). When p14 Y116 phosphorylation is increased in cells with either co-expression of CA c-src or addition of the phosphatase inhibitor pervanadate, GFP-labeled Grb2 co-localized and enriched with p14 at the plasma membrane (***Figure 3e and f***). However, Grb2 did not co-localize or enrich with p14 at the plasma membrane when the Grb2 binding site was mutated to FVAI and co-expressed with CA src or treated with pervanadate (***Figure 3e and f***, and ***Figure 3—figure supplement 1f and g***).

Having shown that Grb2 binds to the p14 cytoplasmic tail in a phosphorylation-dependent manner, we next sought to determine mechanistically how Grb2, an adaptor protein with two SH3 domains, plays a role in p14-mediated cell-cell fusion. The N-terminal SH3 domain of Grb2 binds to SOS, activating Ras, which in turn activates Raf kinase and the MAPK-ERK1/2 pathway, while the C-terminal SH3 domain of Grb2 binds to the actin nucleation promoting factor N-WASP, which binds to Arp2/3 and nucleates branched actin assembly (***Figure 4a***). To determine if one or both pathways are important for fusion, we first treated cells expressing p14 with sorafenib tosylate, an inhibitor of Raf kinase, but found no effect on cell-cell fusion at up to 100 times the IC_{50} (***Figure 4b***). We next considered whether branched actin networks could be directly involved in p14-mediated cell-cell fusion. Building on previous work showing that cytochalasin D disrupts fusion of p14-expressing cells (***Salsman et al., 2008***), we treated p14-expressing cells with wiskostatin, an inhibitor of N-WASP. We found that p14 trafficking to the plasma membrane fusion was unperturbed, but cell-cell fusion was significantly reduced (***Figure 4b***, ***Figure 4—figure supplement 1a and b***). We then treated p14-expressing cells with CK-666 to inhibit the Arp2/3 complex, which nucleates branched actin filaments, and found that fusion was reduced in a dose-dependent manner despite proper trafficking of p14 to the plasma membrane (***Figure 4b***, ***Figure 4—figure supplement 1a and b***). Interestingly, treating p14-expressing cells with smifH2, an inhibitor of formins, enhanced cell-cell fusion (***Figure 4b***), perhaps due to increased branched actin assembly that has been observed when formins are broadly inhibited (***Burke et al., 2014***).

To test whether the reduction in cell-cell fusion with wiskostatin and CK-666 was the result of a direct link between N-WASP and p14 or a more general inhibition of actin activity, we over-expressed Grb2 mutants that can only bind to either SOS or N-WASP by truncating either the N- or C-terminal SH3 domains, respectively. We found that both of these Grb2 mutants bound to p14 WT and co-localized with phosphorylated p14 in pervanadate-treated live cell images (***Figure 4—figure supplement 1c***), confirming that the mutations did not disrupt interactions with p14. However, when the Grb2 N-terminal mutant that can bind only to SOS (Nterm) was over-expressed, the extent of p14-mediated cell-cell fusion was reduced, similar to when endogenous Grb2 binding was reduced by overexpression of the Grb2 SH2 domain (***Figure 4c***, ***Figure 4—figure supplement 1d,e and f***). When a Grb2 C-terminal mutant that can bind only to N-WASP (Cterm) was over-expressed, p14-

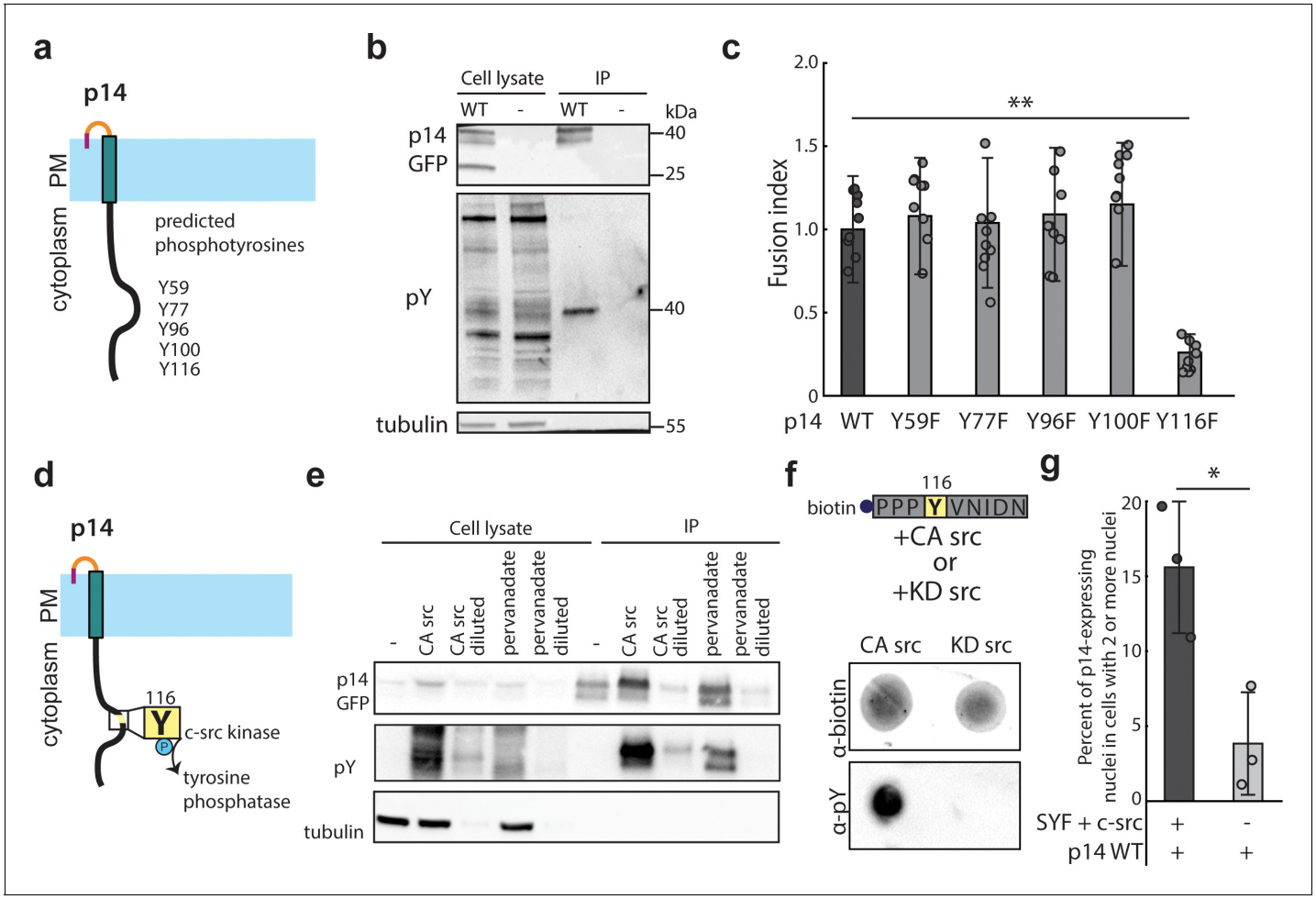

Figure 2. p14 Y116 in the cytoplasmic tail is necessary for cell-cell fusion and is phosphorylated by c-src kinase. (**a**) Schematic of predicted phosphotyrosines in p14 cytoplasmic tail (See also ***Figure 2—figure supplement 1a***). (**b**) Western blot probed with α-phosphotyrosine confirming that p14 WT is phosphorylated. (**c**) Average fusion index of p14 phosphotyrosine mutants with error bars representing standard deviations from 3 independent transfections of 3 wells each. p-values are two-tailed, two-sample Student's t-test where *** = p<0.001 (See also ***Figure 2—figure supplement 1b***). (**d**) Schematic of c-src kinase and a tyrosine phosphatase activity on p14 Y116. (**e**) Western blot probed with α-phosphotyrosine confirming that p14 Y116 phosphorylation is increased with co-expression of constitutively active c-src kinase and with addition of pervanadate. (**f**) Dot blot of p14 cytoplasmic tail peptide phosphorylated *in vitro* with constitutively-active (Y527F) and kinase-dead c-src kinase (Y527F, K295R) (See also ***Figure 2—figure supplement 1c, (d***). (**g**) Average percent of p14-expressing cells with 2 or more nuclei in SYF and SYF + c-src cells with error bars representing standard deviations from 3 independent transfections. p-values are two-tailed, two-sample Student's t-test, where * = p<0.05 (See also ***Figure 2—figure supplement 1e***).

The online version of this article includes the following source data and figure supplement(s) for figure 2:

Source data 1. Excel Spreadsheet of counts for p14-expressing SYF and SYF+c-src cells for ***Figure 2g***.
Figure supplement 1. Characterization of p14 cytoplasmic tail and Y116.

mediated cell-cell fusion was restored to a level comparable to that of endogenous Grb2 in WT cells (***Figure 4c***, ***Figure 4—figure supplement 1d,e and f***). To further confirm the specificity of N-WASP-nucleated branched actin assembly in p14-mediated cell-cell fusion, we expressed p14 WT in N-WASP null (N-WASP -/-) mouse embryonic fibroblasts. We found that the extent of p14-mediated cell-cell fusion was attenuated in N-WASP -/- cells compared to wild-type mouse embryonic fibroblasts (***Figure 4d***, ***Figure 4—figure supplement 1g***).

To determine whether N-WASP binding to Grb2 and the p14 cytoplasmic tail is sufficient to nucleate actin assembly, we used an *in vitro* actin-based motility assay. We bound biotinylated p14 cytoplasmic tail peptides to streptavidin beads in a purified actin motility mixture containing N-WASP (lacking the EVH1 domain), Arp2/3, profilin, cofilin, capping protein and actin,

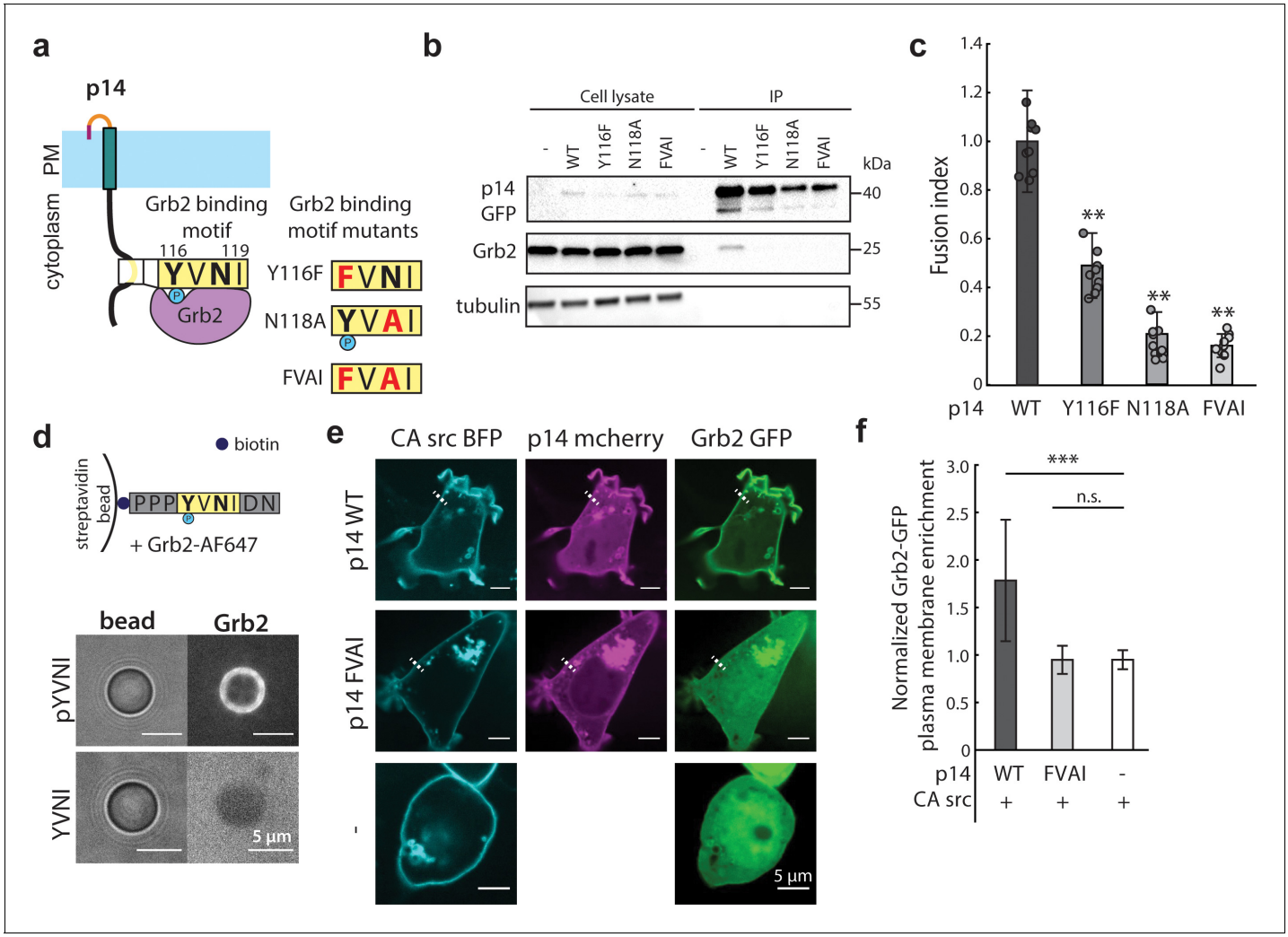

Figure 3. p14 Y116 in the cytoplasmic tail binds to Grb2. (**a**) Schematic of p14 mutants that disrupt predicted Grb2 binding motif. (**b**) Western blot of co-immunoprecipitation of p14 with Grb2 (lane 7) and p14 mutants, Y116F, N118A, FVAI, that does not bind Grb2 (lane 8, 9, 10). (**c**) Average fusion index of p14 mutants with error bars representing standard deviations from 3 independent transfections of 3 wells each. P-values are two-tailed, two-sample Student's t-test where *** = p<0.001 (See also ***Figure 3—figure supplement 1a, (b)***). (**d**) Streptavidin beads with biotinylated phosphorylated and non-phosphorylated Y116 p14 cytoplasmic tail peptide encoding (P113-N121) binds and did not bind to purified Grb2 respectively (See also ***Figure 3—figure supplement 1c, (d)***). (**e**) Confocal images of Grb2-GFP (green) enrichment to the plasma membrane of cells co-expressing p14 WT, p14 FVAI mCherry (magenta) and wildtype HEK293T with constitutively active c-src kinase (cyan). (**f**) Average normalized Grb2-GFP plasma membrane enrichment in cells co-expressing constitutively active c-src and either p14 WT (n = 33 cells) or p14 FVAI (n = 26 cells) or expressing constitutively active c-src alone (n = 24 cells). Error bars represent standard deviations from three independent transfsections. P-values are two-tailed, two-sample Student's t-test where *** = p<0.001 and n.s. = p>0.05.

The online version of this article includes the following source data and figure supplement(s) for figure 3:

Source data 1. Excel Spreadsheet of plasma membrane enrichment of Grb2-GFP in cells expressing CA-src alone or with p14-WT-mcherry or with p14-FVAI mcherry.

Figure supplement 1. Characterization of Grb2 binding to p14.

Figure supplement 1—source data 1. Excel Spreadsheet of surface biotinylation of p14-WT-GFP and p14-FVAI-GFP for ***Figure 3—figure supplement 1a***.

supplemented with Grb2 (***Figure 4—figure supplement 1h***). When Y116 of the p14 cytoplasmic tail peptide was phosphorylated, actin tails were nucleated from the bead (***Figure 4e***), but when Y116 was not phosphorylated, actin tails were not observed (***Figure 4e***). This confirms that Grb2 is necessary and sufficient to recruit N-WASP to the p14 cytoplasmic tail and can nucleate localized branched actin networks when p14 is present.

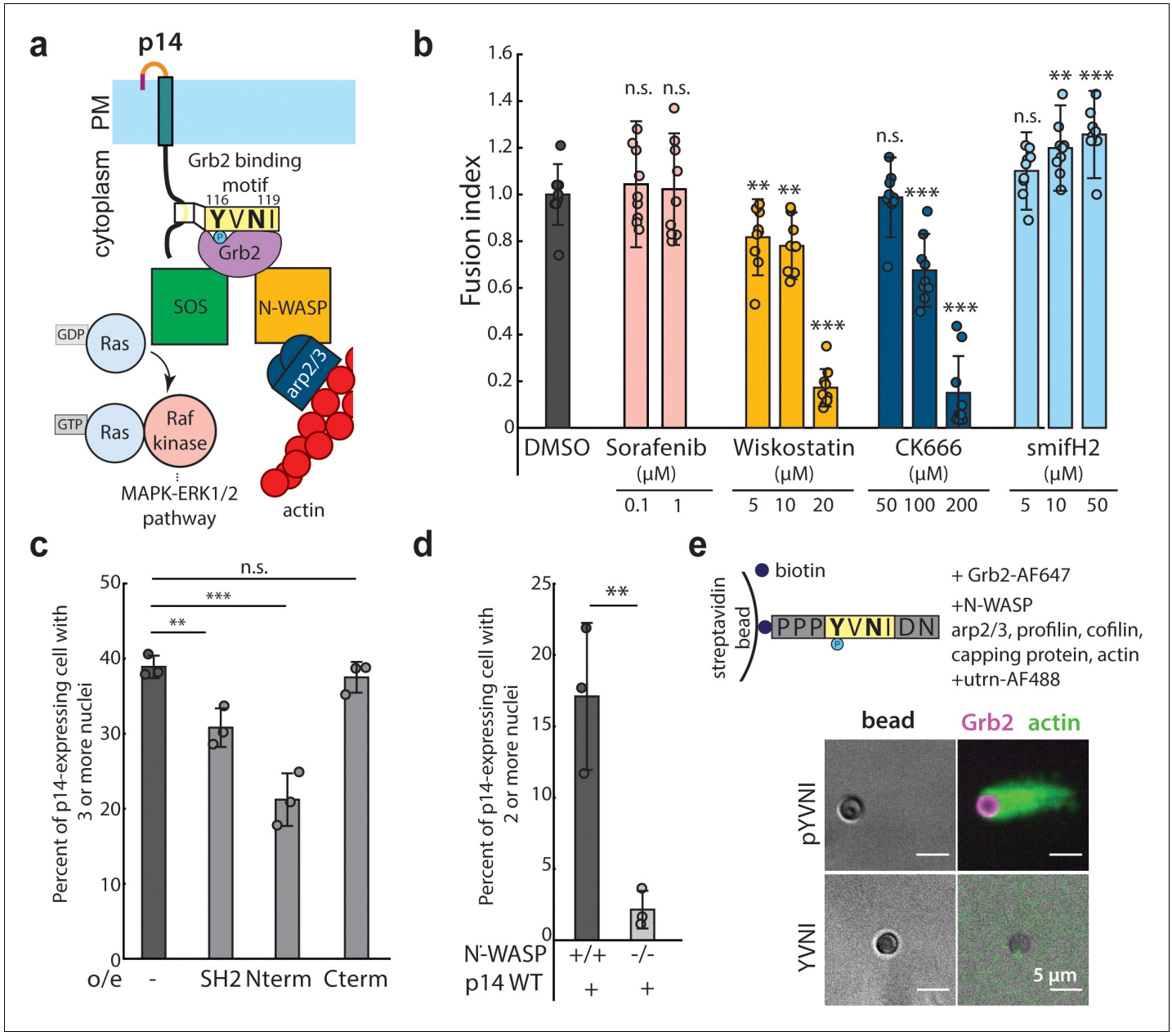

Figure 4. N-WASP-dependent assembly of branched actin network is necessary for cell-cell fusion. (**a**) Schematic of Grb2 binding to two potential downstream effectors, SOS and N-WASP (**b**) Extent of cell-cell fusion quantified with splitYFP fluorescence assay of p14 expressing cells treated sorafenib tosylate targeting Raf kinase, wiskostatin targeting N-WASP, CK-666 targeting Arp2/3 and smifH2 targeting formins, normalized to that of p14 WT treated with vehicle control, DMSO. Error bars indicate standard deviations from 3 independent transfections of 3 wells each. P-values are two-tailed, two-sample Student's t-test to DMSO where ** = p<0.01, *** = p<0.001 and n.s. = p>0.05. (**c**) Average percent of p14-expressing cells with 3 or more nuclei in HEK293T WT cells and HEK293T cells overexpressing Grb2 SH2 domain, N-terminus SH2-SH3 mutant and C-terminus SH2-SH3 mutant. P-values are two-tailed, two-sample Student's t-test where ** = p<0.01, *** = p<0.001 and n.s. = p>0.05. Error bars represent standard deviations from 3 independent transfections (See also ***Figure 4—figure supplement 1a,b,c,d***, and ***Figure 4—source data 1***). (**d**) Average percent of p14-expressing cells with 2 or more nuclei in N-WASP -/- and +/+ cells with error bars representing standard deviations from 3 independent transfections. P-values are two-tailed, two-sample Student's t-test where ** = p<0.01 (See also ***Figure 4—figure supplement 1g***). (**e**) *In vitro* actin bead motility of phosphorylated p14 cytoplasmic tail peptide conjugated to streptavidin beads in a purified actin motility mixture supplemented with Grb2. Polymerized actin is visualized with AlexaFluor488-labeled utrophin actin binding domain (See also ***Figure 4—figure supplement 1h***).

The online version of this article includes the following source data and figure supplement(s) for figure 4:

Source data 1. Excel Spreadsheet of counts and distribution for p14-expressing HEK293T cells over-expressing Grb2 mutants for ***Figure 4c***.
Source data 2. Excel Spreadsheet of counts and distribution for p14-expressing N-WASP -/- or +/+ mouse embryonic fibroblasts for ***Figure 4d***.
Figure supplement 1. Characterization of over-expression of Grb2 mutants and purified components of actin motility assay.

Figure 4 continued on next page

Figure 4 continued

Figure supplement 1—source data 1. Excel Spreadsheet of surface biotinylation of p14-WT-GFP treated with wiskostatin and CK-666 for ***Figure 4—figure supplement 1b***.

We next investigated whether branched actin network assembly must be directly coupled to the fusogenic ectodomain, or whether the fusogenic ectodomain can simply be present in the same membrane as actin assembly by the cytoplasmic tail of p14. To test the necessity for direct coupling, we co-expressed the ectodomain deletion mutant (Δecto; ΔM1-T35), which traffics to the plasma membrane and binds Grb2 (***Figure 5—figure supplement 1a and b***) and the cytoplasmic tail deletion mutant (Δcyto) in the same cell. Interestingly, we found that cell-cell fusion was abolished (***Figure 5a***, and ***Figure 5—figure supplement 1c***), despite the presence of both halves of p14. This indicates that actin assembly localized to the p14 ectodomain is necessary to drive fusion. This also suggests why native Arp2/3-generated branched actin networks at cell-cell contacts (***Efimova and Svitkina, 2018***) are not sufficient to cause spontaneous cell-cell fusion. We note that the mechanism described here is in addition to the role of the actin cytoskeleton at E-cadherin-mediated cell-cell adhesion sites (***Salsman et al., 2008***).

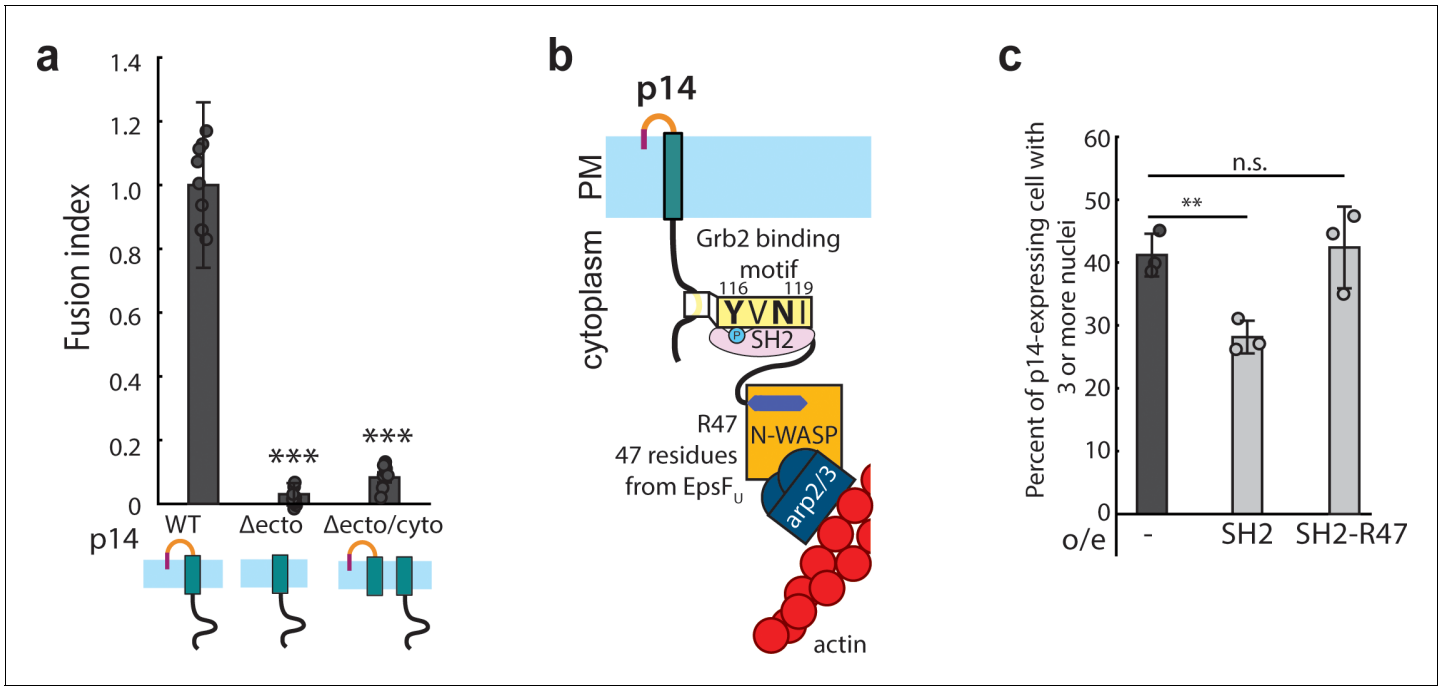

Figure 5. Branched actin assembly directly coupled to p14 cytoplasmic tail drives cell-cell fusion. (**a**) Average fusion index of p14 truncation mutants normalized to that of p14 WT. P-values are two-tailed, two-sample Student's t-test to p14 WT where *** = p<0.001. Error bars indicate standard deviations from 3 independent transfections of 3 wells each (See also ***Figure 5—figure supplement 1a, (b,c)***. (**b**) Schematic of fusion protein coupling actin assembly to p14 cytoplasmic tail consisting of Grb2 SH2 domain and 47 residues from EspF$_U$. (**c**) Average percent of p14-expressing cell with 3 or more nuclei in HEK293T WT cells and HEK293T cells overexpressing Grb2 SH2 domain and SH2-R47. P-values are two-tailed, two-sample Student's t-test where ** = p<0.01 and n.s. = p>0.05. Error bars represent standard deviations from 3 independent transfections (See also ***Figure 5—figure supplement 1d,e,f,g***, and ***Figure 5—source data 1***).

The online version of this article includes the following source data and figure supplement(s) for figure 5:

Source data 1. Excel Spreadsheet of counts and distribution for p14-expressing HEK293T cells over-expressing R47 constructs for ***Figure 5c***.

Figure supplement 1. Characterization of p14 Δectodomain and direct coupling of p14 to actin assembly.

Figure supplement 1—source data 1. Excel Spreadsheet of surface biotinylation of p14-WT-GFP and p14-Δecto-GFP for ***Figure 5—figure supplement 1a***.

Figure supplement 2. Characterization of p14 at time and site of fusion.

Figure supplement 2—source data 1. Excel Spreadsheet of normalized intensity of p14-WT-mCherry and SH2-GFP at fusion site ~200 s prior to fusion for ***Figure 5—figure supplement 2b and d***.

If actin assembly directly coupled to p14 is necessary and sufficient for the fusogenic activity of p14, then it should be possible to drive cell-cell fusion by creating an alternate link between p14 and branched actin network assembly. To test this idea, we engineered a fusion protein that binds to p14 consisting of Grb2 SH2 domain and a 47-residue peptide from $EspF_U$ of enterohemorrhagic *E. coli* (EHEC) (***Figure 5b***). This 47-residue peptide binds to and relieves the auto-inhibition of endogenous N-WASP, nucleating branched actin network (***Cheng et al., 2008***; ***Sallee et al., 2008***). Fusion of this peptide with the Grb2 SH2 domain, which we confirmed binds to phosphorylated p14 (***Figure 5—figure supplement 1d***), enables binding to WT p14. When we expressed this fusion protein (SH2-R47) together with p14 in HEK293T, cell-cell fusion was significantly higher than when the SH2 domain lacking R47 was expressed to a similar level (***Figure 5c***, ***Figure 5—figure supplement 1e,f and g***). This result demonstrates that direct coupling of branched actin assembly to p14 is necessary and sufficient for fusion.

Discussion

This study reveals how a viral pathogen hijacks branched actin network assembly to drive cell-cell fusion, reminiscent of how the pathogens *Listeria monocytogenes* and vaccinia virus hijack branched actin network assembly to move within and between cells (***Welch and Way, 2013***). Here we show that the reptilian orthoreovirus fusogen p14 accomplishes this by presenting a c-src kinase substrate in its cytoplasmic tail, binding the host cell adaptor protein Grb2, and initiating branched actin assembly through the host nucleation promoting factor N-WASP. Since p14 ectodomain extends only 0.7–1.5 nm from the plasma membrane (***Corcoran et al., 2006***), it cannot interact with apposing membrane through the ~2 nm repulsive hydration barrier. If that barrier can be overcome, for example by using divalent cations to bring bare membranes containing negatively charged PS together *in vitro*, the p14 ectodomain is able to disrupt and mix membranes (***Top et al., 2005***). However, it is unclear how such close membrane-membrane interaction is achieved on the crowded plasma membrane where the lipid bilayer is sterically blocked by dense membrane proteins.

We propose that the primary role of branched actin network assembly by p14 is to physically push the fusogenic ectodomain into the opposing plasma membrane, a step normally carried out by conformational changes of tall fusogens. In this model, localized force generation by branched actin network assembly around p14's cytoplasmic domain drives close membrane apposition by coupling to and pushing against the cortical actin cytoskeleton, much like other actin-based membrane protrusions. This close apposition in the presence of p14's membrane-disruptive ectodomain, which contains hydrophobic residues and myristoylation that are known to be necessary for fusion (***Corcoran et al., 2004***; ***Corcoran and Duncan, 2004***; ***Top et al., 2009***), may be sufficient to drive cell-cell fusion. Several other roles of the actin cytoskeleton may also be important for p14-bsaed cell-cell fusion. The actin cytoskeleton could promote clustering of p14 ectodomains into sub-diffraction-limited domains (***Köster and Mayor, 2016***), although enrichment of p14 or phosphorylated p14 was not readily observed at sites of fusion (***Figure 5—figure supplement 2a,b,c and d***). The actin cytoskeleton could also change local membrane curvature and tension (***Kozlov and Chernomordik, 2015***), block fusion pore closure, and/or actively expand the fusion pore (***Kozlov and Chernomordik, 2015***), all of which would promote cell-cell fusion by p14.

Membrane fusion driven by other fusogens has long implicated the actin cytoskeleton (***Kondo et al., 2015***; ***Sanderson et al., 1998***). The proposed roles of the actin cytoskeleton include regulating the activity, localization and enrichment of fusogens at fusion sites (***Yang et al., 2017***), regulating protein-protein interactions (***Wakimoto et al., 2013***), and enlarging the fusion pore (***Wurth et al., 2010***; ***Zheng and Chang, 1990***). In cases where the putative fusogen remains unidentified or the mechanism of fusion remains unclear, the actin cytoskeleton has been suggested as a key player. Examples include formation of signaling scaffolds and protrusive structures during osteoclast fusion (***Oikawa et al., 2012***), macrophage fusion (***Faust et al., 2019***), and myoblast fusion in *Drosophila* (***Kim et al., 2015***; ***Sens et al., 2010***). Protrusive membrane structures generated by branched actin assembly have also been observed at fusogenic synapses (***Shilagardi et al., 2013***) and can be formed *in vitro* (***Liu et al., 2008a***; ***Simon et al., 2019***).

Our findings may be relevant to putative fusogens like myomixer, a short extracellular peptide that is required for myoblast fusion (***Bi et al., 2018***; ***Leikina et al., 2018***; ***Millay et al., 2013***; ***Quinn et al., 2017***; ***Sampath et al., 2018***; ***Zhang et al., 2017***) and does not resemble

conformational-change based fusogens. Like p14, myomixer, together with its partner myomaker, could harness the actin cytoskeleton to drive cell-cell fusion by physically forcing a short fusogenic ectodomain through dense cell surface proteins and into contact with an apposing membrane. In this model of cell-cell fusion, local forces generated by the cytoskeleton, rather than by conformational changes in a tall fusogen, provide a powerful tool for cells and pathogens to create multinucleated structures.

Materials and methods

Cloning

Reptilian reovirus membrane fusion protein, p14 (Accession number: Q80FJ1), was synthesized and inserted into mammalian expression vector pcDNA3.1 with C-terminus tags (mcherry, eGFP). Point mutations and truncations were introduced with primers.

splitYFPa and splitYFPb were amplified from pBiFC-bJun-YN155 and pBiFC-bFos-YC155 (a kind gift from Tom Kerppola) and inserted into lentiviral transfer plasmid, pHR, with Gibson assembly.

Constitutively active chick-src kinase was amplified from pLNCX chick src Y527F and inserted into pcDNA 3.1 with linker (GGGS) and C-terminus tags (FLAG and mTagBFP2). pLNCX chick src Y527F was a gift from Joan Brugge (Addgene plasmid # 13660). K295R was introduced to constitutive active chick-src kinase to render it kinase dead with primers. cDNA of Human Grb2 (GE Dharmacon, cloneID: 3345524) was amplified and inserted into pGEX4T2 with a N-terminus GST tag and TEV cleavage site for purification of Grb2. For overexpression of Grb2 mutants, IRES Puromycin was amplified from pLV-EF1a-IRES-Puro (a gift from Tobias Meyer, Addgene plasmid #85132) and inserted into lentiviral pHR backbone to create pHR-IRES-Puro. Grb2 N-terminus SH3 domain and SH2 domain (N-termSH3, 1–159), Grb2 C-terminus SH3 domain and SH2 domain (C-termSH3, 58–217), and Grb2 SH2 domain (58-159) were amplified from cDNA of Human Grb2 and inserted into pHR-IRES-Puro with C terminus FLAG tag.

47 residues from $EspF_U$ of enterohemorrhagic *E. coli* (268–314) was synthesized and inserted with GGGS linker downstream of Grb2 SH2 domain (58-159) and FLAG tag into pHR-IRES-Puro.

Cell culture, transfection and generation of mutant Grb2 overexpression cells

HEK293T cells were obtained from UCSF Cell Culture Facility. SYF (CRL-2459) and SYF + c-src (CRL-2498) cells were obtained from ATCC. N-WASP -/- and +/+ mouse embryonic fibroblasts were a kind gift from Scott Snapper. All cells were grown in DMEM (Life Technologies) supplemented with 10% heat-inactivated FBS (Life Technologies) and 1% Pen-Strep (Life Technologies), at 37˚C, 5% CO_2. Cells were negative for mycoplasma as verified with Mycoalert mycoplasma detection kit (Lonza).

Cells were transfected with TransIT-293 (Mirus Bio) according to manufacturer's instructions.

To over-express Grb2 mutants to compete with endogenously expressed Grb2 and SH2 actin nucleators, pHR-Grb2NtermSH3-FLAG-IRES-Puro, pHR-Grb2CtermSH3-FLAG-IRES-Puro, pHR-Grb2SH2-FLAG-IRES-Puro, pHR-SH2-FLAG-R47 were co-transfected with second generation packaging plasmids, pMD2.G and p8.91 in HEK293T to generate lentivirus.

HEK293T cells were transduced with lentivirus, and 24 hr post transduction selected with 3 µg/ml puromycin (Clontech) to select for mutant Grb2 expression. Cultures were maintained in 3 µg/ml puromycin.

splitYFP cell-cell fusion assay pHR-splitYFPa and pHR-splitYFPb were co-transfected with second generation packaging plasmids, pMD2.G and p8.91 in HEK293T to generate lentivirus. WT HEK293T cells were transduced with splitYFPa and splitYFPb lentivirus. The cells were passaged for at least a week before use in cell-cell fusion assay.

To quantify cell-cell fusion, HEK293T cells stably expressing splitYFPa and splitYFPb were mixed at 50:50 ratios and 1.33×10^5 of cells were plated into each well of 48 well plate. The next day, the cells were transfected with TransitIT-293 (Mirus Bio). 18 hr post transfection, cells were moved to 30˚C, 5% CO_2 incubator to mature the splitYFP fluorophore. 24 hr post transfection, cells were lifted with 150 µl of 2 mM EDTA and placed into 96 well black bottom plate. splitYFP was excited at 510 nm and emission at 530 nm was quantified using a plate reader (Tecan).

Fusion index was quantified as $(I_{sample} - I_{cell}) / (I_{p14WT} - I_{cell})$, where I_{cell} is the YFP intensity of non-transfected HEK293T cells expressing splitYFPa and splitYFPb, I_{sample} is the YFP intensity of HEK293T cells transfected with plasmid as specified, I_{p14WT} is the YFP intensity of HEK293T cells transfected with p14 WT and treated with DMSO as vehicle control. Average and standard deviation of fusion index is calculated from 3 independent transfections of 3 wells each. Statistical significance was determined using two-tailed, two-sample Student's t-test.

Nuclei count

3.8×10^5 cells were plated into 24 well plates and transfected the next day with designated plasmid with TransIT-293 (Mirus Bio) according to manufacturer's instructions. 2 hr post transfection, cells were lifted with 150 µl of 2 mM EDTA, re-suspended with 850 µl of media, and 300 µl of cell suspension was plated onto a fibronectin-coated glass bottom chamber (Cell-vis). At 6 hr and 18 hr post transfection, cells were transferred to 30˚C, 5% CO_2 incubator. After 6 hr incubation at 30˚C, nuclei were labeled with 0.6% Hoechst 33342 (Life Technologies), and plasma membrane were labeled with 0.05% CellMask Deep Red (Thermo Fisher Scientific) for 20 min at 37˚C. Cells were imaged using spinning disk confocal microscopy. About 80–100 random field of views are taken for each sample to image almost the entire imaging well, and the number of nuclei in p14 expressing cells are manually counted. Average and standard deviation of binned nuclei count is calculated from 3 independent transfections. Statistical significance was determined using two-tailed, two-sample Student's t-test. Statistical significance between distributions of nuclei in p14-expressing cells were determined using Kolmogorov–Smirnov test (ks-test).

Drug treatment

To broadly inhibit the protein-tyrosine phosphatases, pervanadate is prepared by incubating 10 mM sodium orthovanadate with 0.15% hydrogen peroxide in 20 mM HEPES for 5 min at room temperature. Pervanadate is neutralized with catalase and added to cells immediately. For western blot, cells were lysed 10 mins after pervanadate addition, for live-imaging, cells were imaged immediately after pervanadate addition.

To perturb the actin cytoskeleton, 4 hr post transfection, the media was replaced with complete media supplemented with cytoskeletal drugs CK-666 (Sigma Aldrich), Wiskostatin (Krackeler Scientific) and smifH2 (EMD Millipore) at specified concentrations. DMSO was used as vehicle control. 18 hr post transfection, splitYFP was matured at 30˚C. At 24 hr post transfection splitYFP fluorescence was quantified as described above.

To inhibit Raf kinase, 4 hr post transfection, the media was replaced with compete media supplemented with sorafenib tosylate (Selleckchem). DMSO was used as a vehicle control. 18 hr post transfection, splitYFP was matured at 30˚C. At 24 hr post transfection splitYFP fluorescence was quantified as described above.

Co-immunoprecipitation

HEK293T were transfected with specified plasmids. 17–24 hr post transfection, HEK293T cells were washed with 1 mM $CaCl_2$/PBS, lifted off the dish with 2 mM EDTA/PBS, pelleted and lysed by incubating in lysis buffer (150 mM NaCl, 25 mM HEPES, 1 mM EDTA, 0.5% NP-40, 1x PhosSTOP phosphatase inhibitor (Roche), 1x HALT protease inhibitor (Thermo Fisher Scientific) for 30 min, and bath sonicated in ice for 3 min. Cell debris was pelleted at 18,000 rcf for 10 min. Cell lysate were precleared with 15 µl of GFP-Trap (Chromotek) for 30 min at 4˚C, and incubated with 15 µl of fresh GFP-Trap beads overnight at 4˚C. The beads were washed with lysis buffer five times, before boiled in Laemmli sample buffer and separated on 4–20% acrylamide gradient gels by SDS-PAGE. Proteins were transferred onto nitrocellulose membrane and probed with primary antibodies, α-Grb2 (1:5000, Clone 81/Grb2, BD Biosciences), α-tubulin (1:5000, Clone YL1/2, Thermo), α-pTyr (1:2000, Phospho-Tyrosine (P-Tyr-1000) MultiMab Rabbit mAb mix #8954, Cell Signaling Technology), α-GFP (1:10000, Clone 3E6, Life Technologies or 1:5000, A21312, Life Technologies), and secondary antibodies, α-mouse HRP (1:10,000, Upstate Biotechnology or 1:5000, Jackson Labs), α-rabbit HRP (1:5000, 65–6120, Thermo Fisher), α-rat AlexaFluor 647 (1:5000, Life Technologies). Western blots were imaged on ChemiDoc (Bio-Rad).

Membrane fractionation

HEK293T were transfected with p14 WT, p14 Y116F/N118A, and p14 Δcyto. 18 hr post transfection, the cells were washed with 1 mM $CaCl_2$/PBS, lifted off the dish with 2 mM EDTA/PBS. Cells were pelleted at 200 rcf for 5 min and re-suspended in fractionation buffer (20 mM HEPES, 10 mM KCl, $MgCl_2$, 1 mM EDTA, 1 mM EGTA, 1 mM TCEP, 1x HALT protease inhibitor(Thermo Fisher Scientific)). The cell suspension lysed with five freeze/thaw cycles. Nuclei were pelleted via centrifugation (700 rcf, 5 min), and mitochondria were pelleted at 10,000 rcf, 5 min. The supernatant was then centrifuged at 100,000 rcf for an hour at 4˚C to separate the membrane and cytoplasmic fraction. The membrane pellet was washed once in fractionation buffer and re-centrifuged at 100,000 rcf for an hour. The cell lysate, cytoplasmic fraction, and membrane pellet was boiled in Laemmli sample buffer, and separated on 4–20% acrylamide gradient gels by SDS-PAGE. Proteins were transferred onto nitrocellulose membrane and probed with primary antibodies, α-tubulin (1:5000, Clone YL1/2, Thermo Fisher Scientific), α-GFP (1:5000, A-21312, Life Technologies), and secondary antibodies, α-rabbit HRP (1:5000, 65–6120, Thermo Fisher) and α-rat AlexaFluor 647 (1:5000, Life Technologies). Western blots were imaged on a ChemiDoc (Bio-Rad).

Surface biotinylation

HEK293T cells were transfected with GFP tagged p14 WT, p14 FVAI, p14 Δcyto, p14 Δecto. P14 WT expressing cells were treated with 20 μM Wiskostatin or 100 μM CK-666 9 hr post transfection. 18–24 hr post transfection, cells were washed with 1 mM CaCl2/PBS on ice, lifted off the dish with ice-cold 2 mM EDTA/PBS. Cells were pelleted at 200 rcf for 5 min and washed with PBS (pH = 8) three times on ice and incubated with 1 mg NHS-Biotin in 0.5 mL PBS (pH = 8) for 1 hr on ice. The biotinylation reaction was quenched with 100 mM glycine in PBS for 10 min at room temperature. Cells were washed three times with 100 mM glycine in PBS and lysed with 1 mL lysis buffer (1x RIPA buffer supplemented with 1x HALT protease inhibitor (Thermo Fisher Scientific)) for 30 min on ice and sonicated for 3 min. Cell debris was pelleted for 5 min at 17,900 rcf at 4˚C. 30 μl of streptavidin magnetic beads (ThermoFisher) were washed with RIPA buffer at 4˚C, the supernatant was added and incubated overnight. Beads were washed 5 times with RIPA buffer, suspended in Laemmli sample buffer (30 ul), denatured at 95˚C for 5 min and separated on 4–20% acrylamide gradient gels by SDS-PAGE. Proteins were transferred onto nitrocellulose membrane with iBlot (Thermo Fisher Scientific). The membrane was blocked with 5% milk powder in TBST for 1 hr and probed with primary antibodies α-GFP (1:5000, g1544, Sigma Aldrich), α-tubulin (1:5000, Clone YL1/2, Thermo) in 5% milk in TBST overnight at 4˚C. The membrane was then probed with secondary antibodies, α-rabbit HRP (1:5000, 65–6120, Thermo Fisher) and, α-rat AlexaFluor 647 (1:5000, Life Technologies). Western blots were imaged on ChemiDoc (Bio-Rad).

Protein purification

GST-TEV-Grb2 (human) was expressed and purified from *E. coli* as previously described (***Su et al., 2016***).

N-WASP (ΔEVH1) was a kind gift from D. Wong and J. Taunton (University of California, San Francisco). Actin was purified from rabbit skeletal muscle as previously described (***Spudich and Watt, 1971***). Capping protein was a kind gift from S. Hansen and D. Mullins (University of California, San Francisco). Arp2/3 was purchased from Cytoskeleton, Inc Profilin, cofilin, and utrophin actin binding domain (1-261) were purified as previously described (***Bieling et al., 2016***; ***Harris et al., 2019***).

Motility assay

Similar to a previously described motility assay (***Okrut et al., 2015***), 2 μl of 0.5% 3 μm streptavidin polystyrene beads (Bangs Laboratories) are incubated with 1 μM biotin-p14 cytoplasmic tail peptide in 10 mM HEPES (pH 7.5), 1 mg/ml BSA and 50 mM KCl for 10 min at room temperature. Peptide-coated beads are diluted eight-fold into motility buffer (10 mM HEPES, 2 mM MgCl2, 50 mM KCl, 50 mM NaCl, 1 mg/ml BSA, 2.5 mM ATP, 5 mM TCEP), containing 0.1 μM Grb2 (20% labeled), 0.2 μM N-WASP, 9 μM actin, 0.075 μM arp2/3, 0.05 μM capping protein, 2.6 μM profilin, 3.5 μM cofilin and incubated for 15 min at room temperature while rotating. 300 nM utrophin-AF488 is added to the mixture, and incubated for 5 min, before imaging.

In vitro kinase assay

As previously described (***Dagliyan et al., 2016***), HEK293T is transiently transfected with constitutively active chick src (Y527F) kinase and kinase dead (Y527F/K295R) src kinase with C-terminus FLAG tag with TransIT-293 (Mirus). 24 hr post transfection, cells were washed with 1 mM $CaCl_2$/PBS, and lifted with 2 mM EDTA. Cells were pelleted, and lysed in 20 mM HEPES-KOH, 50 mM KCl, 100 mM NaCl, 1 mM EGTA, 1% NP-40, 1x PhosSTOP phosphatase inhibitor (Roche) and 1x HALT protease inhibitor (Thermo Scientific) for 30 min, 4˚C while rotating. Cell debris was pelleted at 3000 g, 10 min, and FLAG-tagged kinase were immunoprecipitated with 3 µg of α-FLAG (M2 clone, Sigma) and 50 µl of Protein-G Dynabeads (Thermo Scientific) for 2 hr, 4˚C, while rotating. Beads were washed twice with intracellular buffer (20 mM HEPES-KOH, 50 mM KCl, 100 mM NaCl, 1 mM EDTA, 1% NP-40), and twice with kinase buffer (25 mM HEPES, 5 mM $MgCl_2$, 5 mM $MnCl_2$, 0.5 mM EGTA). Beads were re-suspended in kinase buffer, supplemented with 0.2 mM ATP and 1.5 mM biotin-p14 cytoplasmic tail peptide, and incubated for 1 hr at room temperature. Protein-G dynabeads were removed, and the supernatant is incubated with 10 µl streptavidin magnetic beads (Pierce) for 30 min, room temperature. Streptavidin magnetic beads were washed twice with kinase buffer, and boiled in sample buffer. Sample are dotted onto nitrocellulose membrane (Bio-Rad), and blocked with 5% BSA, and probed with α-pTyr (1:5000, Phospho-Tyrosine (P-Tyr-1000) MultiMab Rabbit mAb mix #8954, Cell Signaling Technology) and α-biotin-AF647 (1:5000, BK-1/39, Santa Cruz Biotechnology) in 5% BSA overnight at 4˚C. Blots were washed 3 times, 5 min each with TBST, and probed with secondary antibody, α-rabbit HRP (1:5000, 65–6120, Thermo Fisher) and washed 3 times, 15 min each. Blots were imaged on Chemi-Doc (Bio-rad).

Imaging

All live cells were maintained at 37˚C, 5% CO_2 with a stage top incubator (okolab) during imaging.

For confocal microscopy, cells were imaged with a spinning disk confocal microscope (Eclipse Ti, Nikon) with a spinning disk (Yokogawa CSU-X, Andor), CMOS camera (Zyla, Andor), and either a 4x objective (Plano Apo, 0.2NA, Nikon) or a 60x objective (Apo TIRF, 1.49NA, oil, Nikon). For total internal reflection fluorescence (TIRF) microscopy, cells were imaged with TIRF microscope (Eclipse Ti, Nikon), 60x objective (Apo TIRF, 1.49NA, oil, Nikon) and EMCCD camera (iXON Ultra, Andor). Both microscopes were controlled with Micro-Manager. Images were analyzed and prepared using ImageJ (National Institutes of Health).

Plasma membrane enrichment of Grb2

HEK293T cells were transfected with either constitutively active (CA) c-src-mTagBFP2 and Grb2-GFP alone, or together and mCherry tagged p14 WT or p14 FVAI. 18–24 hr post transfection, HEK293T cells were imaged with spinning disk confocal microscope with a 60x objective (Apo TIRF, 1.49NA, oil, Nikon). CA c-src BFP localizes to the plasma membrane and was used as a plasma membrane marker. Grb2-GFP fluorescence intensity at the plasma membrane was normalized to its fluorescence intensity at the cytoplasm in cells expressing either CA-src alone or together with p14 WT and p14 FVAI. The average normalized Grb2 enrichment at the plasma membrane from three independent transfections were compared.

Acknowledgements

The authors would like to thank R Duncan and E Chen for helpful discussion and the Fletcher Lab members, including MH Bakalar, BD Belardi, AR Harris, and MD Vahey, for useful feedback and technical consultation.

Additional information

Funding

Funder	Grant reference number	Author
National Institute of General Medical Sciences	R01GM114671	Daniel A Fletcher

Chan Zuckerberg Biohub	Investigator Award	Daniel A Fletcher
National Science Foundation	DBI-1548297	Daniel A Fletcher
National Science Foundation	GRFP	Ka Man Carmen Chan
Life Sciences Research Foundation		Sungmin Son

The funders had no role in study design, data collection and interpretation, or the decision to submit the work for publication.

Author contributions

Ka Man Carmen Chan, Conceptualization, Resources, Formal analysis, Validation, Investigation, Visualization, Methodology, Writing - original draft, Writing - review and editing; Sungmin Son, Conceptualization, Funding acquisition, Investigation, Methodology, Writing - review and editing; Eva M Schmid, Conceptualization, Funding acquisition, Writing - review and editing; Daniel A Fletcher, Conceptualization, Supervision, Funding acquisition, Writing - original draft, Project administration, Writing - review and editing

Author ORCIDs

Ka Man Carmen Chan https://orcid.org/0000-0002-8595-9725
Daniel A Fletcher https://orcid.org/0000-0002-1890-5364

Decision letter and Author response

Decision letter https://doi.org/10.7554/eLife.51358.sa1
Author response https://doi.org/10.7554/eLife.51358.sa2

Additional files

Supplementary files

- Supplementary file 1. Key resources table.
- Transparent reporting form

Data availability

All data generated or analysed during this study are included in the manuscript and supporting files.

References

Bi P, McAnally JR, Shelton JM, Sánchez-Ortiz E, Bassel-Duby R, Olson EN. 2018. Fusogenic micropeptide myomixer is essential for satellite cell fusion and muscle regeneration. *PNAS* **115**:3864–3869. DOI: https://doi.org/10.1073/pnas.1800052115, PMID: 29581287

Bieling P, Li TD, Weichsel J, McGorty R, Jreij P, Huang B, Fletcher DA, Mullins RD. 2016. Force feedback controls motor activity and mechanical properties of Self-Assembling branched actin networks. *Cell* **164**:115–127. DOI: https://doi.org/10.1016/j.cell.2015.11.057, PMID: 26771487

Blom N, Sicheritz-Pontén T, Gupta R, Gammeltoft S, Brunak S. 2004. Prediction of post-translational glycosylation and phosphorylation of proteins from the amino acid sequence. *Proteomics* **4**:1633–1649. DOI: https://doi.org/10.1002/pmic.200300771, PMID: 15174133

Bullough PA, Hughson FM, Skehel JJ, Wiley DC. 1994. Structure of influenza haemagglutinin at the pH of membrane fusion. *Nature* **371**:37–43. DOI: https://doi.org/10.1038/371037a0, PMID: 8072525

Burke TA, Christensen JR, Barone E, Suarez C, Sirotkin V, Kovar DR. 2014. Homeostatic actin cytoskeleton networks are regulated by assembly factor competition for monomers. *Current Biology* **24**:579–585. DOI: https://doi.org/10.1016/j.cub.2014.01.072, PMID: 24560576

Chen J, Skehel JJ, Wiley DC. 1999. N- and C-terminal residues combine in the fusion-pH influenza hemagglutinin HA(2) subunit to form an N cap that terminates the triple-stranded coiled coil. *PNAS* **96**:8967–8972. DOI: https://doi.org/10.1073/pnas.96.16.8967, PMID: 10430879

Cheng HC, Skehan BM, Campellone KG, Leong JM, Rosen MK. 2008. Structural mechanism of WASP activation by the enterohaemorrhagic *E. coli* effector EspF(U). *Nature* **454**:1009–1013. DOI: https://doi.org/10.1038/nature07160, PMID: 18650809

Chernomordik LV, Kozlov MM. 2003. Protein-lipid interplay in fusion and fission of biological membranes. *Annual Review of Biochemistry* **72**:175–207. DOI: https://doi.org/10.1146/annurev.biochem.72.121801.161504, PMID: 14527322

Ciechonska M, Duncan R. 2014. Reovirus FAST proteins: virus-encoded cellular fusogens. *Trends in Microbiology* **22**:715–724. DOI: https://doi.org/10.1016/j.tim.2014.08.005, PMID: 25245455

Compton AA, Schwartz O. 2017. They might be giants: does syncytium formation sink or spread HIV infection? *PLOS Pathogens* **13**:e1006099. DOI: https://doi.org/10.1371/journal.ppat.1006099, PMID: 28152024

Corcoran JA, Syvitski R, Top D, Epand RM, Epand RF, Jakeman D, Duncan R. 2004. Myristoylation, a protruding loop, and structural plasticity are essential features of a nonenveloped virus fusion peptide motif. *Journal of Biological Chemistry* **279**:51386–51394. DOI: https://doi.org/10.1074/jbc.M406990200, PMID: 15448165

Corcoran JA, Salsman J, de Antueno R, Touhami A, Jericho MH, Clancy EK, Duncan R. 2006. The p14 fusion-associated small transmembrane (FAST) protein effects membrane fusion from a subset of membrane microdomains. *Journal of Biological Chemistry* **281**:31778–31789. DOI: https://doi.org/10.1074/jbc.M602566200, PMID: 16936325

Corcoran JA, Duncan R. 2004. Reptilian reovirus utilizes a small type III protein with an external myristylated amino terminus to mediate cell-cell fusion. *Journal of Virology* **78**:4342–4351. DOI: https://doi.org/10.1128/JVI.78.8.4342-4351.2004, PMID: 15047847

Dagliyan O, Tarnawski M, Chu PH, Shirvanyants D, Schlichting I, Dokholyan NV, Hahn KM. 2016. Engineering extrinsic disorder to control protein activity in living cells. *Science* **354**:1441–1444. DOI: https://doi.org/10.1126/science.aah3404, PMID: 27980211

Dawe S, Duncan R. 2002. The S4 genome segment of baboon reovirus is bicistronic and encodes a novel fusion-associated small transmembrane protein. *Journal of Virology* **76**:2131–2140. DOI: https://doi.org/10.1128/jvi.76.5.2131-2140.2002, PMID: 11836390

Dinkel H, Van Roey K, Michael S, Kumar M, Uyar B, Altenberg B, Milchevskaya V, Schneider M, Kühn H, Behrendt A, Dahl SL, Damerell V, Diebel S, Kalman S, Klein S, Knudsen AC, Mäder C, Merrill S, Staudt A, Thiel V, et al. 2016. ELM 2016–data update and new functionality of the eukaryotic linear motif resource. *Nucleic Acids Research* **44**:D294–D300. DOI: https://doi.org/10.1093/nar/gkv1291, PMID: 26615199

Domachowske JB, Rosenberg HF. 1999. Respiratory syncytial virus infection: immune response, immunopathogenesis, and treatment. *Clinical Microbiology Reviews* **12**:298–309. DOI: https://doi.org/10.1128/CMR.12.2.298, PMID: 10194461

Duncan R, Murphy FA, Mirkovic RR. 1995. Characterization of a novel syncytium-inducing baboon reovirus. *Virology* **212**:752–756. DOI: https://doi.org/10.1006/viro.1995.1536, PMID: 7571448

Duncan R, Corcoran J, Shou J, Stoltz D. 2004. Reptilian reovirus: a new fusogenic Orthoreovirus species. *Virology* **319**:131–140. DOI: https://doi.org/10.1016/j.virol.2003.10.025, PMID: 14967494

Efimova N, Svitkina TM. 2018. Branched actin networks push against each other at Adherens junctions to maintain cell-cell adhesion. *Journal of Cell Biology* **217**:1827–1845. DOI: https://doi.org/10.1083/jcb.201708103, PMID: 29507127

Faust JJ, Balabiyev A, Heddleston JM, Podolnikova NP, Baluch DP, Chew TL, Ugarova TP. 2019. An actin-based protrusion originating from a podosome-enriched region initiates macrophage fusion. *Molecular Biology of the Cell* **30**:2254–2267. DOI: https://doi.org/10.1091/mbc.E19-01-0009, PMID: 31242090

Fédry J, Liu Y, Péhau-Arnaudet G, Pei J, Li W, Tortorici MA, Traincard F, Meola A, Bricogne G, Grishin NV, Snell WJ, Rey FA, Krey T. 2017. The ancient gamete fusogen HAP2 is a eukaryotic class II fusion protein. *Cell* **168**:904–915. DOI: https://doi.org/10.1016/j.cell.2017.01.024, PMID: 28235200

Feng J, Dong X, Pinello J, Zhang J, Lu C, Iacob RE, Engen JR, Snell WJ, Springer TA. 2018. Fusion surface structure, function, and dynamics of gamete fusogen HAP2. *eLife* **7**:e39772. DOI: https://doi.org/10.7554/eLife.39772, PMID: 30281023

Gong R, Peng X, Kang S, Feng H, Huang J, Zhang W, Lin D, Tien P, Xiao G. 2005. Structural characterization of the fusion core in Syncytin, envelope protein of human endogenous retrovirus family W. *Biochemical and Biophysical Research Communications* **331**:1193–1200. DOI: https://doi.org/10.1016/j.bbrc.2005.04.032, PMID: 15883002

Guo H, Sun X, Yan L, Shao L, Fang Q. 2013. The NS16 protein of aquareovirus-C is a fusion-associated small transmembrane (FAST) protein, and its activity can be enhanced by the nonstructural protein NS26. *Virus Research* **171**:129–137. DOI: https://doi.org/10.1016/j.virusres.2012.11.011, PMID: 23201583

Harris AR, Belardi B, Jreij P, Wei K, Shams H, Bausch A, Fletcher DA. 2019. Steric regulation of tandem calponin homology domain actin-binding affinity. *Molecular Biology of the Cell* **30**:3112–3122. DOI: https://doi.org/10.1091/mbc.E19-06-0317, PMID: 31693446

Harrison SC. 2015. Viral membrane fusion. *Virology* **479-480**:498–507. DOI: https://doi.org/10.1016/j.virol.2015.03.043, PMID: 25866377

Ivanovic T, Harrison SC. 2015. Distinct functional determinants of influenza hemagglutinin-mediated membrane fusion. *eLife* **4**:e11009. DOI: https://doi.org/10.7554/eLife.11009, PMID: 26613408

Kim JH, Ren Y, Ng WP, Li S, Son S, Kee YS, Zhang S, Zhang G, Fletcher DA, Robinson DN, Chen EH. 2015. Mechanical tension drives cell membrane fusion. *Developmental Cell* **32**:561–573. DOI: https://doi.org/10.1016/j.devcel.2015.01.005, PMID: 25684354

Kondo N, Marin M, Kim JH, Desai TM, Melikyan GB. 2015. Distinct requirements for HIV-cell fusion and HIV-mediated cell-cell fusion. *Journal of Biological Chemistry* **290**:6558–6573. DOI: https://doi.org/10.1074/jbc.M114.623181, PMID: 25589785

Köster DV, Mayor S. 2016. Cortical actin and the plasma membrane: inextricably intertwined. *Current Opinion in Cell Biology* **38**:81–89. DOI: https://doi.org/10.1016/j.ceb.2016.02.021, PMID: 26986983

Kozlov MM, Chernomordik LV. 2015. Membrane tension and membrane fusion. *Current Opinion in Structural Biology* **33**:61–67. DOI: https://doi.org/10.1016/j.sbi.2015.07.010, PMID: 26282924

Leikina E, Gamage DG, Prasad V, Goykhberg J, Crowe M, Diao J, Kozlov MM, Chernomordik LV, Millay DP. 2018. Myomaker and myomerger work independently to control distinct steps of membrane remodeling during myoblast fusion. *Developmental Cell* **46**:767–780. DOI: https://doi.org/10.1016/j.devcel.2018.08.006, PMID: 30197239

Liu AP, Richmond DL, Maibaum L, Pronk S, Geissler PL, Fletcher DA. 2008a. Membrane-induced bundling of actin filaments. *Nature Physics* **4**:789–793. DOI: https://doi.org/10.1038/nphys1071, PMID: 19746192

Liu Y, Tewari R, Ning J, Blagborough AM, Garbom S, Pei J, Grishin NV, Steele RE, Sinden RE, Snell WJ, Billker O. 2008b. The conserved plant sterility gene HAP2 functions after attachment of fusogenic membranes in Chlamydomonas and plasmodium gametes. *Genes & Development* **22**:1051–1068. DOI: https://doi.org/10.1101/gad.1656508, PMID: 18367645

Millay DP, O'Rourke JR, Sutherland LB, Bezprozvannaya S, Shelton JM, Bassel-Duby R, Olson EN. 2013. Myomaker is a membrane activator of myoblast fusion and muscle formation. *Nature* **499**:301–305. DOI: https://doi.org/10.1038/nature12343, PMID: 23868259

Mohler WA, Shemer G, del Campo JJ, Valansi C, Opoku-Serebuoh E, Scranton V, Assaf N, White JG, Podbilewicz B. 2002. The type I membrane protein EFF-1 is essential for developmental cell fusion. *Developmental Cell* **2**:355–362. DOI: https://doi.org/10.1016/S1534-5807(02)00129-6, PMID: 11879640

Mori T, Kuroiwa H, Higashiyama T, Kuroiwa T. 2006. GENERATIVE CELL SPECIFIC 1 is essential for angiosperm fertilization. *Nature Cell Biology* **8**:64–71. DOI: https://doi.org/10.1038/ncb1345, PMID: 16378100

Moss B. 2006. Poxvirus entry and membrane fusion. *Virology* **344**:48–54. DOI: https://doi.org/10.1016/j.virol.2005.09.037, PMID: 16364735

Obenauer JC, Cantley LC, Yaffe MB. 2003. Scansite 2.0: proteome-wide prediction of cell signaling interactions using short sequence motifs. *Nucleic Acids Research* **31**:3635–3641. DOI: https://doi.org/10.1093/nar/gkg584, PMID: 12824383

Oikawa T, Oyama M, Kozuka-Hata H, Uehara S, Udagawa N, Saya H, Matsuo K. 2012. Tks5-dependent formation of circumferential podosomes/invadopodia mediates cell-cell fusion. *The Journal of Cell Biology* **197**:553–568. DOI: https://doi.org/10.1083/jcb.201111116, PMID: 22584907

Okrut J, Prakash S, Wu Q, Kelly MJ, Taunton J. 2015. Allosteric N-WASP activation by an inter-SH3 domain Linker in nck. *PNAS* **112**:E6436–E6445. DOI: https://doi.org/10.1073/pnas.1510876112, PMID: 26554011

Pancera M, Zhou T, Druz A, Georgiev IS, Soto C, Gorman J, Huang J, Acharya P, Chuang GY, Ofek G, Stewart-Jones GB, Stuckey J, Bailer RT, Joyce MG, Louder MK, Tumba N, Yang Y, Zhang B, Cohen MS, Haynes BF, et al. 2014. Structure and immune recognition of trimeric pre-fusion HIV-1 env. *Nature* **514**:455–461. DOI: https://doi.org/10.1038/nature13808, PMID: 25296255

Parmar HB, Barry C, Duncan R. 2014. Polybasic trafficking signal mediates golgi export, ER retention or ER export and retrieval based on membrane-proximity. *PLOS ONE* **9**:e94194. DOI: https://doi.org/10.1371/journal.pone.0094194, PMID: 24714640

Pérez-Vargas J, Krey T, Valansi C, Avinoam O, Haouz A, Jamin M, Raveh-Barak H, Podbilewicz B, Rey FA. 2014. Structural basis of eukaryotic cell-cell fusion. *Cell* **157**:407–419. DOI: https://doi.org/10.1016/j.cell.2014.02.020, PMID: 24725407

Podbilewicz B. 2014. Virus and cell fusion mechanisms. *Annual Review of Cell and Developmental Biology* **30**:111–139. DOI: https://doi.org/10.1146/annurev-cellbio-101512-122422, PMID: 25000995

Quinn ME, Goh Q, Kurosaka M, Gamage DG, Petrany MJ, Prasad V, Millay DP. 2017. Myomerger induces fusion of non-fusogenic cells and is required for skeletal muscle development. *Nature Communications* **8**:15665. DOI: https://doi.org/10.1038/ncomms15665, PMID: 28569755

Racine T, Hurst T, Barry C, Shou J, Kibenge F, Duncan R. 2009. Aquareovirus effects syncytiogenesis by using a novel member of the FAST protein family translated from a noncanonical translation start site. *Journal of Virology* **83**:5951–5955. DOI: https://doi.org/10.1128/JVI.00171-09, PMID: 19297495

Rand RP, Parsegian VA. 1989. Hydration forces between phospholipid bilayers. *Biochimica Et Biophysica Acta (BBA) - Reviews on Biomembranes* **988**:351–376. DOI: https://doi.org/10.1016/0304-4157(89)90010-5

Renard M, Varela PF, Letzelter C, Duquerroy S, Rey FA, Heidmann T. 2005. Crystal structure of a pivotal domain of human syncytin-2, a 40 million years old endogenous retrovirus fusogenic envelope gene captured by primates. *Journal of Molecular Biology* **352**:1029–1034. DOI: https://doi.org/10.1016/j.jmb.2005.07.058, PMID: 16140326

Sallee NA, Rivera GM, Dueber JE, Vasilescu D, Mullins RD, Mayer BJ, Lim WA. 2008. The pathogen protein EspF (U) hijacks actin polymerization using mimicry and multivalency. *Nature* **454**:1005–1008. DOI: https://doi.org/10.1038/nature07170, PMID: 18650806

Salsman J, Top D, Barry C, Duncan R. 2008. A virus-encoded cell-cell fusion machine dependent on surrogate adhesins. *PLOS Pathogens* **4**:e1000016. DOI: https://doi.org/10.1371/journal.ppat.1000016, PMID: 18369467

Sampath SC, Sampath SC, Millay DP. 2018. Myoblast fusion confusion: the resolution begins. *Skeletal Muscle* **8**:3. DOI: https://doi.org/10.1186/s13395-017-0149-3, PMID: 29386054

Sanderson CM, Frischknecht F, Way M, Hollinshead M, Smith GL. 1998. Roles of vaccinia virus EEV-specific proteins in intracellular actin tail formation and low pH-induced cell-cell fusion. *Journal of General Virology* **79**:1415–1425. DOI: https://doi.org/10.1099/0022-1317-79-6-1415, PMID: 9634084

Sapir A, Avinoam O, Podbilewicz B, Chernomordik LV. 2008. Viral and developmental cell fusion mechanisms: conservation and divergence. *Developmental Cell* **14**:11–21. DOI: https://doi.org/10.1016/j.devcel.2007.12.008, PMID: 18194649

Sens KL, Zhang S, Jin P, Duan R, Zhang G, Luo F, Parachini L, Chen EH. 2010. An invasive podosome-like structure promotes fusion pore formation during myoblast fusion. *The Journal of Cell Biology* **191**:1013–1027. DOI: https://doi.org/10.1083/jcb.201006006, PMID: 21098115

Shemer G, Suissa M, Kolotuev I, Nguyen KC, Hall DH, Podbilewicz B. 2004. EFF-1 is sufficient to initiate and execute tissue-specific cell fusion in *C. elegans*. *Current Biology* **14**:1587–1591. DOI: https://doi.org/10.1016/j.cub.2004.07.059, PMID: 15341747

Shilagardi K, Li S, Luo F, Marikar F, Duan R, Jin P, Kim JH, Murnen K, Chen EH. 2013. Actin-propelled invasive membrane protrusions promote fusogenic protein engagement during cell-cell fusion. *Science* **340**:359–363. DOI: https://doi.org/10.1126/science.1234781, PMID: 23470732

Shmulevitz M, Epand RF, Epand RM, Duncan R. 2004. Structural and functional properties of an unusual internal fusion peptide in a nonenveloped virus membrane fusion protein. *Journal of Virology* **78**:2808–2818. DOI: https://doi.org/10.1128/JVI.78.6.2808-2818.2004, PMID: 14990700

Shmulevitz M, Duncan R. 2000. A new class of fusion-associated small transmembrane (FAST) proteins encoded by the non-enveloped fusogenic Reoviruses. *The EMBO Journal* **19**:902–912. DOI: https://doi.org/10.1093/emboj/19.5.902, PMID: 10698932

Simon C, Kusters R, Caorsi V, Allard A, Abou-Ghali M, Manzi J, Di Cicco A, Lévy D, Lenz M, Joanny J-F, Campillo C, Plastino J, Sens P, Sykes C. 2019. Actin dynamics drive cell-like membrane deformation. *Nature Physics* **15**:602–609. DOI: https://doi.org/10.1038/s41567-019-0464-1

Smith EC, Popa A, Chang A, Masante C, Dutch RE. 2009. Viral entry mechanisms: the increasing diversity of paramyxovirus entry. *FEBS Journal* **276**:7217–7227. DOI: https://doi.org/10.1111/j.1742-4658.2009.07401.x, PMID: 19878307

Spudich JA, Watt S. 1971. The regulation of rabbit skeletal muscle contraction. I. biochemical studies of the interaction of the tropomyosin-troponin complex with actin and the proteolytic fragments of myosin. *The Journal of Biological Chemistry* **246**:4866–4871. PMID: 4254541

Su X, Ditlev JA, Hui E, Xing W, Banjade S, Okrut J, King DS, Taunton J, Rosen MK, Vale RD. 2016. Phase separation of signaling molecules promotes T cell receptor signal transduction. *Science* **352**:595–599. DOI: https://doi.org/10.1126/science.aad9964, PMID: 27056844

Südhof TC, Rothman JE. 2009. Membrane fusion: grappling with SNARE and SM proteins. *Science* **323**:474–477. DOI: https://doi.org/10.1126/science.1161748, PMID: 19164740

Top D, de Antueno R, Salsman J, Corcoran J, Mader J, Hoskin D, Touhami A, Jericho MH, Duncan R. 2005. Liposome reconstitution of a minimal protein-mediated membrane fusion machine. *The EMBO Journal* **24**:2980–2988. DOI: https://doi.org/10.1038/sj.emboj.7600767, PMID: 16079913

Top D, Barry C, Racine T, Ellis CL, Duncan R. 2009. Enhanced fusion pore expansion mediated by the trans-acting endodomain of the reovirus FAST proteins. *PLOS Pathogens* **5**:e1000331. DOI: https://doi.org/10.1371/journal.ppat.1000331, PMID: 19266079

Valansi C, Moi D, Leikina E, Matveev E, Graña M, Chernomordik LV, Romero H, Aguilar PS, Podbilewicz B. 2017. *Arabidopsis* HAP2/GCS1 is a gamete fusion protein homologous to somatic and viral fusogens. *Journal of Cell Biology* **216**:571–581. DOI: https://doi.org/10.1083/jcb.201610093, PMID: 28137780

von Besser K, Frank AC, Johnson MA, Preuss D. 2006. Arabidopsis HAP2 (GCS1) is a sperm-specific gene required for pollen tube guidance and fertilization. *Development* **133**:4761–4769. DOI: https://doi.org/10.1242/dev.02683, PMID: 17079265

Wakimoto H, Shimodo M, Satoh Y, Kitagawa Y, Takeuchi K, Gotoh B, Itoh M. 2013. F-actin modulates measles virus cell-cell fusion and assembly by altering the interaction between the matrix protein and the cytoplasmic tail of hemagglutinin. *Journal of Virology* **87**:1974–1984. DOI: https://doi.org/10.1128/JVI.02371-12, PMID: 23221571

Welch MD, Way M. 2013. Arp2/3-mediated actin-based motility: a tail of pathogen abuse. *Cell Host & Microbe* **14**:242–255. DOI: https://doi.org/10.1016/j.chom.2013.08.011, PMID: 24034611

Wilcox GE, Compans RW. 1982. Cell fusion induced by Nelson bay virus. *Virology* **123**:312–322. DOI: https://doi.org/10.1016/0042-6822(82)90264-1, PMID: 6294979

Wilson IA, Skehel JJ, Wiley DC. 1981. Structure of the haemagglutinin membrane glycoprotein of influenza virus at 3 A resolution. *Nature* **289**:366–373. DOI: https://doi.org/10.1038/289366a0, PMID: 7464906

Wurth MA, Schowalter RM, Smith EC, Moncman CL, Dutch RE, McCann RO. 2010. The actin cytoskeleton inhibits pore expansion during PIV5 fusion protein-promoted cell-cell fusion. *Virology* **404**:117–126. DOI: https://doi.org/10.1016/j.virol.2010.04.024, PMID: 20537366

Yang Y, Zhang Y, Li WJ, Jiang Y, Zhu Z, Hu H, Li W, Wu JW, Wang ZX, Dong MQ, Huang S, Ou G. 2017. Spectraplakin induces positive feedback between fusogens and the actin cytoskeleton to promote Cell-Cell fusion. *Developmental Cell* **41**:107–120. DOI: https://doi.org/10.1016/j.devcel.2017.03.006, PMID: 28399395

Zeev-Ben-Mordehai T, Vasishtan D, Siebert CA, Grünewald K. 2014. The full-length cell-cell fusogen EFF-1 is monomeric and upright on the membrane. *Nature Communications* **5**:3912. DOI: https://doi.org/10.1038/ncomms4912, PMID: 24867324

Zhang Q, Vashisht AA, O'Rourke J, Corbel SY, Moran R, Romero A, Miraglia L, Zhang J, Durrant E, Schmedt C, Sampath SC, Sampath SC. 2017. The microprotein minion controls cell fusion and muscle formation. *Nature Communications* **8**:15664. DOI: https://doi.org/10.1038/ncomms15664, PMID: 28569745

Zheng QA, Chang DC. 1990. Dynamic changes of microtubule and actin structures in CV-1 cells during electrofusion. *Cell Motility and the Cytoskeleton* **17**:345–355. DOI: https://doi.org/10.1002/cm.970170409, PMID: 2076549